WPPMI-CPR(17) 17578

B Koncar et al.

Heat Loads and Design Temperature Optimization of DEMO Thermal Shields

Preprint of Paper to be submitted for publication in Proceeding of 13th International Symposium on Fusion Nuclear Technology (ISFNT)

This work has been carried out within the framework of the EUROfusion Consortium and has received funding from the Euratom research and training programme 2014-2018 under grant agreement No 633053. The views and opinions expressed herein do not necessarily reflect those of the European Commission.

This document is intended for publication in the open literature. It is made available on the clear understanding that it may not be further circulated and extracts or references may not be published prior to publication of the original when applicable, or without the consent of the Publications Officer, EUROfusion Programme Management Unit, Culham Science Centre, Abingdon, Oxon, OX14 3DB, UK or e-mail Publications.Officer@euro-fusion.org

Enquiries about Copyright and reproduction should be addressed to the Publications Officer, EUROfusion Programme Management Unit, Culham Science Centre, Abingdon, Oxon, OX14 3DB, UK or e-mail Publications.Officer@euro-fusion.org

The contents of this preprint and all other EUROfusion Preprints, Reports and Conference Papers are available to view online free at http://www.euro-fusionscipub.org. This site has full search facilities and e-mail alert options. In the JET specific papers the diagrams contained within the PDFs on this site are hyperlinked

Heat Loads and Design Temperature Optimization of DEMO Thermal Shields

Boštjan Končar[a], Martin Draksler[a], Richard Brown[b], Christian Bachmann[b]

[a]*Jožef Stefan Institute, Reactor Engineering Division*
[b]*PPPT, PMU, Eurofusion*

The initial concept of DEMO thermal shields is analyzed, based on the static heat loads evaluation and optimization of thermal shields design temperature. Evaluation of heat loads involve thermal analysis of thermal shields and superconducting magnets. Thermal radiation between the surfaces and heat conduction loads due to physical contacts are considered. The influence of thermal shields temperature on the refrigeration power of the cryogenic system is analyzed. Sensitivity studies have been performed aiming to improve the efficiency of thermal shielding and reduce the total refrigeration power. The effects of the following parameters were analyzed: vacuum vessel operating temperature, possibility of independent cooling loops for vacuum vessel and cryostat thermal shields and inclusion of additional passive thermal radiation shields.

Keywords: thermal shields, DEMO, heat loads, refrigeration power, temperature optimization.

1. Introduction

The superconducting magnets in DEMO will be cooled by helium at about 4 K and enclosed between the hot vacuum vessel, with operational temperature of 200 °C, and the cryostat at room temperature. Thermal shields will be used to protect the magnet system from the thermal radiation transferred from the vacuum vessel and the cryostat. To effectively reduce thermal radiation, thermal shields should have surfaces with low emissivity and should be actively cooled in the temperature range between 80 K and 120 K [1][2].

The concept of DEMO thermal shields is analyzed and optimized, based on thermal analysis of static heat loads and reduction of the refrigeration power required to actively cool the magnets and thermal shields. Analysis of static heat loads takes into account the thermal radiation between component surfaces and heat conduction losses at the component supports. In terms of reducing the refrigeration power, a series of sensitivity cases have been performed to study the influence of vacuum vessel temperature, thermal shields temperature optimisation and the effect of additional passive thermal shields.

2. Calculation methods

The present study evaluates static heat loads on the thermal shields and superconducting magnets located in the interspace between the vacuum vessel and the cryostat. The accumulated heat is removed by active cooling system connected to the cryogenic plant. The heat loads are calculated by analytical methods, which have been prior validated by numerical simulations on the real DEMO tokamak geometry [3],[4]. Operating temperature of the thermal shields influences the heat load distribution and affects the total refrigeration power of the cryogenic system. Optimal temperature of the thermal shields is sought to minimize the refrigeration power.

2.1 Heat load calculations

Steady-state heat loads include thermal radiation exchange between the hot surfaces (vacuum vessel (VV) and cryostat) and cold surfaces (thermal shields and magnets) and heat conduction losses through the various supports and attachments.

In high vacuum conditions of the cryostat and at high temperature differences between the hot and cold component surfaces, thermal radiation represents one of the main contributions to the overall heat load. Nuclear heating is not considered in the present analysis though it may importantly affect the heat load on magnets [5]. The relative effect on thermal shields is not expected to be high. In the ITER case [6] the neutron heating contributes to about 1% of the heat load on the thermal shields. The expected influence of nuclear heating on the total heat load and consequently on the refrigeration power can be important, but it will not affect the optimal configuration and temperature of thermal shields discussed in the present study.

Thermal radiation exchange (in Watts) between the hot and cold surfaces A_h and A_c at temperatures T_h, T_c with surface emissivities $\varepsilon_h, \varepsilon_c$, can be calculated as:

$$Q^{rad} = \sigma \cdot A_c \cdot \varepsilon_r \cdot \left(T_h^4 - T_c^4 \right), \tag{1}$$

where σ is the Stefan-Boltzmann constant and ε_r is the relative emissivity between the surfaces. In the case of cold magnets shielded by the vacuum vessel thermal shield (VVTS) and the cryostat thermal shield (CTS) at equal temperature T_h, the relative emissivity is defined as:

$$\varepsilon_r = \frac{1}{\frac{1}{\varepsilon_c} + \left(\frac{1}{\varepsilon_h} - 1 \right) \frac{A_c}{(A_h)}}, \tag{2}$$

Relative emissivity can be simplified for the large,

Corresponding author: Bostjan.Koncar@ijs.si

approximately similar surfaces ($A_h = A_c$¿that are placed together at a small distance:

$$\varepsilon_r = \frac{1}{\frac{1}{\varepsilon_c} + \frac{1}{\varepsilon_h} - 1}. \quad (3)$$

The relation (3) describes the relative emissivity between the vacuum vessel and VVTS and between the cryostat and CTS.

Heat conduction loads at the components supports and attachments are described by the Fourier law:

$$Q_{\square}^{cnd} = A_{cnd} \cdot \frac{1}{L_{cnd}} \cdot \int_{Tc}^{Th} k(T)\, dT, \quad (4)$$

where A_{cnd} is the contact area, L_{cnd} is the conductive length between the cold and hot component and $k(T)$ is the temperature dependent thermal conductivity of the material [7]. Heat conduction losses occur at the VVTS and CTS supports. VVTS is attached directly to the toroidal magnet field coils (TFC), while CTS is supported from the cryostat. The highest heat conduction losses can be expected through the gravity supports (GS), which support the heavy TFC magnets. Direct heat conduction between the cryostat pedestal ring and TFC is reduced by the thermal anchor, which removes part of the conducted heat through the CTS cooling system [8]. Details on individual heat load calculations are given in [9].

Table 1 summarizes the calculated thermal radiation and heat conduction contributions at normal operating conditions. It is assumed that at DEMO normal operation the vacuum vessel and superconducting magnets operate at 473 K and 4 K, respectively [10],[11]. Both thermal shields (VVTS and CTS) are cooled to the same working temperature of 80 K. This set of boundary conditions in Table 1 denotes the "base case". Temperatures of the components and heat load sources are listed in the first two columns of Table 1, calculated heat loads on the magnets and thermal shields are collected in adjacent columns. It can be seen that VVTS intercepts more than 80% of the total heat load (912.6 kW) owing to the thermal radiation from the vacuum vessel. The heat load on the CTS is nearly five times lower (189.4 kW) with thermal radiation being the main contributor. Heat conduction through the gravity supports (38.4 kW) also presents a substantial portion of the total CTS heat load. Heat conduction between the thermal anchor at 80 K and TFC at 4K is the largest contributor to the total magnets heat load (~6 kW). Though the heat load on the magnets is rather low comparing to the thermal shields, it requires high refrigeration power for its removal to the ambient. Note, that DEMO thermal shielding concept is similar to the ITER one [13].

2.2 Theoretical refrigeration power

The heat intercepted by the thermal shields and magnets has to be removed through the refrigeration process. The minimum theoretical power required to pump the heat from a cold temperature T_c to the heat sink at higher ambient temperature T_{amb} (293K) can be written as follows [12]:

$$P_i = Q_i \cdot \frac{(T_{amb} - T_c)}{T_c}, \quad (5)$$

where P_i and Q_i denote theoretical refrigeration power and heat load of i-th cooled component, respectively. The ratio $(T_{amb} - T_c)/T_c$ in Eq. (5) is the Carnot factor that defines the refrigeration cost of an ideal cooling cycle. Namely, in an ideal case a minimum 72.2 W of power would be needed to remove 1W of heat (Carnot factor 72.2) from the magnets at T_c=4K. For cooling of the thermal shields (T_c=80K), merely 2.6 W would be sufficient. The total power for cooling of all components (VVTS, CTS and magnets) is defined as the sum of individual refrigeration powers ($P_{tot} = \sum P_i$). Due to the inevitable entropy losses, the refrigeration power in the real cryoplant may be up to 5 times higher than the theoretical value. The mechanical efficiency of the cryoplant depends on the cryogenic process and thermo-hydraulic parameters of the cryogenic loop [12].

Table 1: Estimated total heat loads on magnets, VVTS and CTS due to thermal radiation and heat conduction (base case)

Temperatures T_{hot}/T_{cold}	Heat load source	Magnets heat load	VVTS heat load	CTS heat load	Total heat load
473 K / 80 K	Thermal radiation from VV	/	912.8 kW	/	
293 K / 80 K	Thermal radiation from cryostat	/	/	149.5 kW	
80 K / 4 K	Thermal radiation form VVTS and CTS to magnets	1.3 kW	/	/	
293 K / 80 K	Gravity supports heat conduction	/	/	38.4 kW	
80 K / 4 K	Thermal anchor heat conduction	4.4 kW	/	/	

Corresponding author: Bostjan.Koncar@ijs.si

80 K / 4 K 293 K / 80 K	VVTS supports heat conduction CTS support heat conduction	0.2 kW /	-0.2 kW /	/ 1.5 KW	
Total heat load		5.9 kW	912.6 kW	189.4 kW	1,107.9 kW

3. Results and discussion

The heat load distributions on the magnets and thermal shields at varied thermal shields working temperatures are discussed first. Second, the sensitivity analyses are performed, which evaluate the effects of separate cooling of the CTS and VVTS, VV operating temperature and additional passive thermal radiation shielding on the refrigeration power.

3.1 Heat load distributions

Variation of heat load distribution on the magnets thermal shields over the range of thermal shield temperatures is presented in Fig. 1 and Fig. 2. Other operating and boundary conditions are the same as in Table 1 (base case). Note that the analysis assumes equal temperatures of the VVTS and CTS ($T_{vvts}=T_{cts}$). It can be seen that the heat load contributions to the magnets in Fig. 1 increase with thermal shield temperature T_{vvts}. For a thermal shield temperature of 100K the radiation heat load on the magnets is 3.3 kW and the heat conduction load on the magnets is around 6 kW (0.32 kW from VVTS supports and 5.6 kW from thermal anchor) which is still considered as reasonably low. The maximum thermal shield operating temperature is therefore recommended to be around 100K. At T_{vvts} around 120 K the thermal radiation contribution Q_{rad} (6.7 kW) surpasses the heat conduction to the magnets.

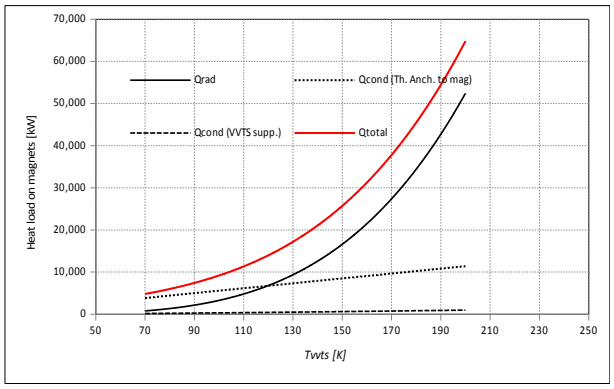

Fig. 1: Heat load contributions on magnets.

On the contrary, heat loads to the VVTS and CTS decrease moderately with rising T_{vvts} (see Fig. 2). In general, the total heat load on VVTS and CTS is by two orders of magnitude higher than the heat load intercepted by magnets. Thermal radiation to the VVTS represents the largest heat load contribution. Heat conduction losses due to thermal shield supports and attachments represent only a smaller part of the total thermal shields heat load.

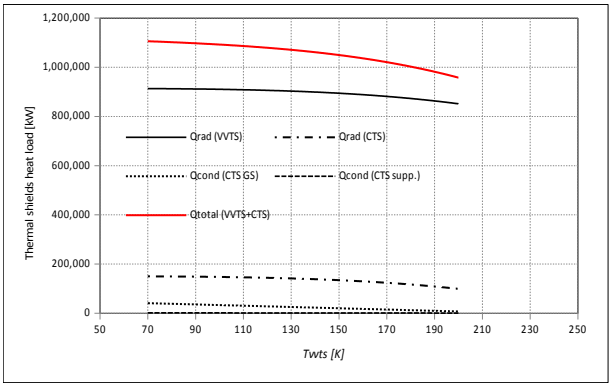

Fig. 2: Heat load contributions to thermal shields.

3.2 Sensitivity analyses to minimize refrigeration power

Heat loads on the thermal shields and magnets have to be removed by the cryogenic system that shall provide helium cooling at different temperature levels. Considering the fixed temperature of the cooled magnets (4 K), it is very useful to found an optimal operating temperatures of VVTS (T_{vvts}) and CTS (T_{cts}), where the total refrigeration power P_{tot} has a minimum value. This is an important step already at the early developmental stage of the thermal shields. Trying to reduce the total refrigeration power, parametric analyses have been performed. The considered sensitivity cases are collected in Table 2. In Cases 2 to 4, the effect of separate VVTS and CTS cooling loops is analysed. Different VV operating temperatures are considered in Cases 5 and 6, whereas the Cases 1-1 to 1-4 analyse the influence of additional passive thermal radiation shields. The main results representing the minimum total refrigeration power $P_{tot(min)}$ at optimal VVTS temperature $T_{vvts(opt)}$ are listed in the last two columns of Table 2.

The variation of refrigeration power with T_{vvts}, for the base case scenario (Case 1 in Table 2) is shown in Fig. 3. In Case 1 equal temperatures of the VVTS and CTS ($T_{vvts}=T_{cts}$) are assumed. The refrigeration power for the magnets P_{mag} is rapidly growing with T_{vvts}. Dashed line representing the refrigeration power of both thermal shields decreases with T_{vvts}. As shown in Fig. 3 and in Table 2, the total refrigeration power reached its minimum at the optimal temperature $T_{vvts(opt)}$=123 K.

Table 2: Parametric cases: minimized total power at optimal VVTS temperature T_{vvts}

Corresponding author: Bostjan.Koncar@ijs.si

		T_{vv} [K]	T_{cts} [K]	VVTS cooling	CTS cooling	$T_{vvts(opt)}$ [K]	$P_{tot(min)}$ [kW]
Base case	Case 1	473	$T_{CTS}=T_{VVTS}$	Active	Active	123	2,563.9
Separate CTS cooling	Case 2	473	80	Active	Active	134	2,455.4
	Case 3	473	60	Active	Active	134	2,602.7
	Case 4	473	150	Active	Active	134	2.789
Varied T_{VV}	Case 5	373	$T_{CTS}=T_{VVTS}$	Active	Active	104	1,684.8
	Case 6	423	$T_{CTS}=T_{VVTS}$	Active	Active	113	2,075.7
Addition of passive radiation shields	Case 1-1	473	$T_{CTS}=T_{VVTS}$	Active	Passive +MLI	134	3,985.3
	Case 1-2	473	$T_{CTS}=T_{VVTS}$	Active	Active +MLI	120	2,433.6
	Case 1-3	473	$T_{CTS}=T_{VVTS}$	Active +MLI	Active	104	1,661.1
	Case 1-4	473	$T_{CTS}=T_{VVTS}$	Active +MLI	Active +MLI	99	1,483.6

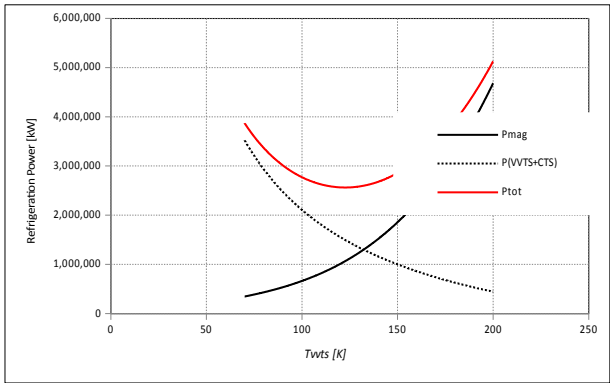

Fig. 3: Dependence of theoretical refrigeration power on the VVTS temperature.

Sensitivity analysis of separate cooling loops for VVTS and CTS is presented in Fig. 4. The temperature T_{vvts} is varied, while the CTS temperature T_{cts} is kept constant at values 80K, 60K and 150K for the Cases 2,3 and 4, respectively. For each of the cases the variation of P_{tot} with T_{vvts} is shown. Comparing to the reference Case 1, P_{tot} is reduced by a small amount (4%) only in the Case 2 (T_{cts}= 80K). The total power is slightly higher for the other two cases. The optimum temperature $T_{vvts(opt)}$is 134 K (see Table 2) for all three cases.

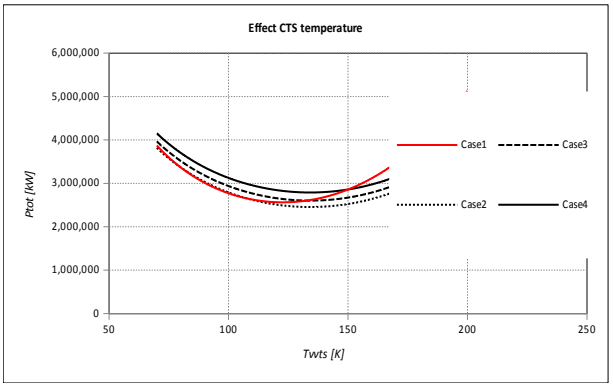

Fig. 4: Influence of separate CTS cooling.

To investigate a wider range of CTS temperatures the variation of minimum refrigeration power $P_{tot(min)}$ with T_{cts} is shown in Fig. 5. Each point on the graph represents the optimal design point for different case. Cases listed in Table 2 are labelled on the graph. Comparison with the base Case 1 shows that separate cooling of CTS cannot significantly reduce $P_{tot(min)}$, hence it does not bring any substantial benefits.

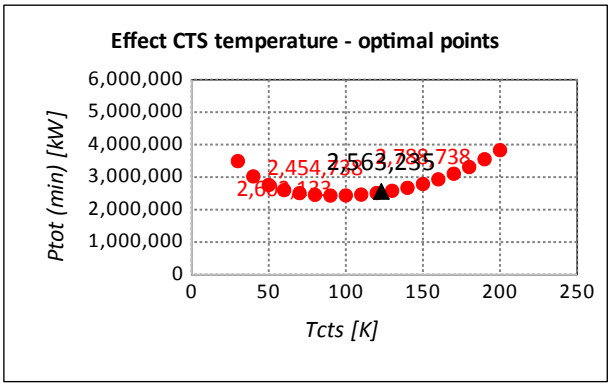

Fig. 5: Influence CTS temperature on the minimum total refrigeration power.

Corresponding author: Bostjan.Koncar@ijs.si

The foreseen VV normal operation temperature of 473 K (Case 1) is beneficial as it avoids regular baking cycles as in ITER [11]. However this substantially increases the heat loads on VVTS and subsequently the total refrigeration power. The cases with lower VV operating temperature (Case 5 and 6) are compared with the base case in Fig. 6. Reduced VV temperature significantly decreases P_{tot} and lowers the optimal temperature $T_{vvts(opt)}$. Decrease of VV temperature from 473 k to 373 K (Case 5) reduces the total refrigeration power by 35% and shifts $T_{vvts(opt)}$ from 123 K to 104 K (see Table 2).

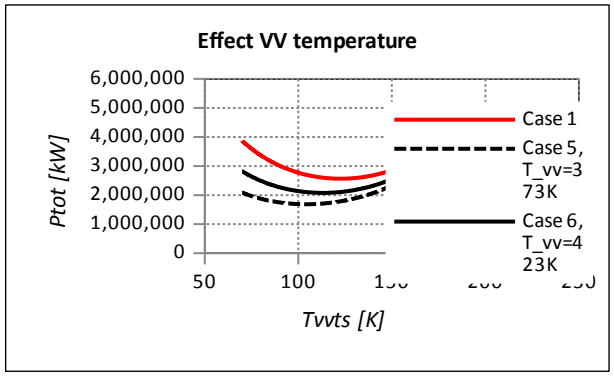

Fig. 6: Influence of vacuum vessel operating temperature.

The influence of additional passive thermal radiation shields is analysed in Fig. 7. In the Case 1-1 the option of having a fully passive CTS is studied. The non-cooled CTS structure is equipped with one passive Multi-Layer-Insulation (MLI) package on the side facing the cryostat. The characteristics of MLI insulation are taken from [14]. One MLI package consists of 20 layers and has the same emissivity as CTS and thermal conductivity of 0.1 W/mK. Compared to the Case 1, the minimum refrigeration power $P_{tot(min)}$ in Case 1-1 is increased by 60%, to nearly 4,000 kW. Such high increase shows that active cooling of the CTS cannot be omitted. In the Case 1-2, MLI is added on the side of actively cooled CTS. Although the $P_{tot(min)}$ is reduced comparing to the Case 1, the reduction is rather small (~5%). Adding of MLI on the side of VVTS (Case 1-3) is much more effective and reduces the $P_{tot(min)}$ by 35%. The optimal temperature $T_{vvts(opt)}$ is lower (104 K) than in the base case (123 K). Addition of MLIs on both thermal shields (Case 1-4) further reduces the $P_{tot(min)}$, but the impact of additional MLI on the CTS side is small comparing to the previous. Comparison of Cases 5 and 1-3 in Table 2 further shows that the influence of reduced VV temperature on the $P_{tot(min)}$ is comparable to the effect of additional passive thermal shield on the side of VVTS.

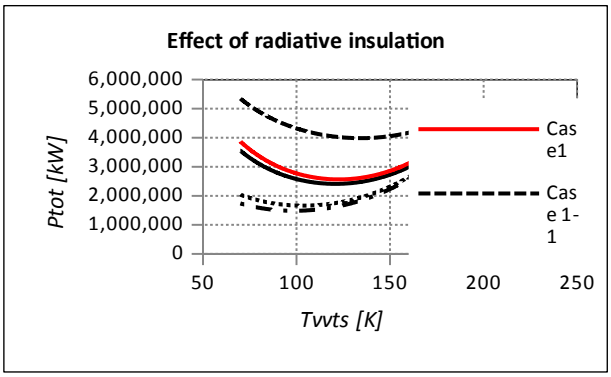

Fig. 7: Influence of additional radiative insulation.

4. Conclusions

Static heat loads on the magnets and thermal shields have been evaluated using the theoretical model. Parametric studies were performed to optimize the operating temperature of the thermal shields and to reduce the refrigeration power of the cryogenic system. The effects of the following parameters were evaluated: vacuum vessel operating temperature, possibility of independent thermal shields cooling loops and passive radiative insulation on the warm side of thermal shields. Main findings are the following:

- Thermal radiation on the VVTS presents the largest contribution to the total heat load (more than 80% at 80 K of thermal shields temperature).
- It is shown that separate cooling of the CTS and VVTS does not bring any substantial benefits to the reduction of refrigeration power. Equal operating temperature of the CTS and VVTS (the same cooling cycle) is therefore recommended.
- The option with passive CTS shows high increase of total refrigeration power, indicating that active CTS cooling cannot be omitted. The actively cooled CTS has a small impact on the total refrigeration power. Inclusion of additional passive shield on the actively cooled CTS does not bring substantial reduction of the total refrigeration power.
- Significantl reduction of the total refrigeration power can be realized by lowering the VV temperature or by additional passive shielding on the side of VVTS. The effect of additional passive thermal shield on the VVTS side is comparable to the effect of reducing the VV temperature from 473K to 373 K. The total theoretical refrigeration power of the base case (2.56 MW) is reduced by 35% in both cases, to approximately 1.66 MW. The optimal thermal shields temperature in both recommended cases is around 100 K and is higher than in the base case (80 K).

Acknowledgments

This work has been carried out within the framework of the EUROfusion Consortium and has received funding from the Euratom research and training programme 2014 - 2018 under grant agreement No 633053. The views and

Corresponding author: Bostjan.Koncar@ijs.si

opinions expressed herein do not necessarily reflect those of the European Commission.

References

[1] M. Wanner et al., Monte Carlo approach to define the refrigerator capacities for JT-60SA, Fusion Eng. Des. 86 (2011) 1511-1513.

[2] K. Nam et al. Thermal analysis on detailed 3D models of ITER thermal shield, Fusion Eng. Des. 89 (2014) 1843-1847.

[3] B. Končar, M. Draksler, O. Costa Garrido, B. Meszaros, Thermal radiation analysis of DEMO tokamak, Fusion Eng. Des. (2017) In Press.

[4] B. Končar, M. Draksler, O. Costa Garrido, I. Vavtar, Thermal analysis of DEMO tokamak 2015, Deliverable PMI-3.2-T03-D01, Jožef Stefan Institute, 2016.

[5] M. Coleman, Advanced definition of neutronic heat load density map on DEMO TF coils, Eurofusion report, July 2016.

[6] C. Hamlyn-Harris et al., Thermal Loads To and From the Thermal Shield, ITER report, April 2011.

[7] V. Barabash, Summary of Material Data For Structural Analysis of the ITER Cryostat, 2010.

[8] M. Coleman, Definition of the external static radiative and conductive heart loads on the TF coil casing. Eurofusion report, Sept. 2016.

[9] B. Končar, M. Draksler, Initial Definition of the DEMO Thermal Shields concept. PMI-6.3-T001-D001, February 2017.

[10] C. Bachmann et al., Initial DEMO tokamak design configuration studies. Fusion Eng Des 98-99 (2015) 1423-1426.

[11] G. Federici et al. European DEMO Design Strategy and Consequences for Materials. Nuclear Fusion (2017) In Press.

[12] T. Flynn, Cryogenic Engineering, 2nd ed., Marcel Dekker, New York, 2005.

[13] C. Hamlyn-Harris et al., System Design Description (DDD) 27 Thermal Shield, June 2014.

[14] M. Nagel, S. Freundt, H. Posselt, Thermal and mechanical analysis of Wendelstein 7-X thermal shield, Fusion Eng. Des. 86 (2011) 1830-1833.

Corresponding author: Bostjan.Koncar@ijs.si